JLB

TECHNICAL ADVANCE

Technical Advance: caspase-1 activation and IL-1β release correlate with the degree of lysosome damage, as illustrated by a novel imaging method to quantify phagolysosome damage

Michael J. Davis and Joel A. Swanson*,†,1*

*Program in Immunology and †Department of Microbiology and Immunology, University of Michigan Medical School, Ann Arbor, Michigan, USA

RECEIVED MARCH 18, 2010; REVISED MAY 21, 2010; ACCEPTED JUNE 5, 2010. DOI: 10.1189/jlb.0310159

ABSTRACT

In addition to the lysosome's important roles in digestion, antigen processing, and microbial destruction, lysosome damage in macrophages can trigger cell death and release of the inflammatory cytokine IL-1β. To examine the relationship among endocytosis, lysosome damage, and subsequent events, such as caspase-1 activation and IL-1β secretion, we developed a method for measuring lysosome disruption inside individual living cells, which quantifies release of Fdx from lysosomes. Unperturbed, cultured BMM exhibited low levels of lysosome damage, which were not increased by stimulation of macropinocytosis. Lysosome damage following phagocytosis differed with different types of ingested particles, with negligible damage after ingestion of sRBC ghosts, intermediate damage by polystyrene (PS) beads, and high levels of damage by ground silica. Pretreatment with LPS decreased the amount of lysosome damage following phagocytosis of PS beads, silica microspheres, or ground silica. Activation of caspase-1 and subsequent release of IL-1β were proportional to lysosome damage following phagocytosis. The low level of damage following PS bead phagocytosis was insufficient to activate caspase-1 in LPS-activated macrophages. These studies indicate that lysosome damage following phagocytosis is dependent on particle composition and dose and that caspase-1 activation and IL-1β secretion correlate with the extent of lysosome damage. *J. Leukoc. Biol.* 88: 813–822; 2010.

Introduction

Lysosomes are membrane-bounded, hydrolase-rich organelles capable of degrading a variety of macromolecules [1, 2] and microbial molecules acquired by fusion with phagosomes, endosomes, or autophagosomes [1, 2]. In macrophages, most phagocytosed microbes are trafficked into lysosomes, killed, and degraded. The luminal space of lysosomes is maintained at pH 4–5 [3], considerably more acidic than the pH neutral cytoplasm that surrounds them. Antigens from exogenous sources are degraded and loaded onto MHC class II molecules in late endosomes and lysosomes [4]. Thus, lysosomes function as the end-point for the endocytic pathway and the major cellular recycling compartment for internalized macromolecules.

Some pathogenic microorganisms evade trafficking into lysosomes through various mechanisms [5], including escape from the endocytic pathway into the host cell cytoplasm. These can be detected by cytosolic recognition systems, such as the NLR family. Upon recognition of microbial molecules, NLR proteins self-associate into oligomeric structures, which can multimerize further with adaptor proteins. These inflammasomes [6] activate inflammatory caspases, mainly caspase-1, which catalyze the proteolytic activation of pro-IL-1β and pro-IL-18 [7]. Although the mechanism of IL-1β secretion is incompletely understood [8], IL-1β maturation is critical for its function [9, 10].

Inflammasomes containing NLRP3, also known as NALP-3, can be activated by conditions that damage cells, so-called "danger signals". Three naturally occurring danger signals—monosodium-urate crystals [11], extracellular ATP [12, 13], and plasma membrane perforation [12, 13], as well as particulate asbestos [14], β-amyloids [15], silica [14, 16, 17], and alum [17, 18]—activate the NLRP3 inflammasome. The NLRP3 inflammasome activity is also triggered by dilution of intracellular potassium, which is a consequence of damage to plasma membranes [19].

Abbreviations: BMM=murine bone marrow-derived macrophages, CCD=charged-coupled device, ex.=excitation, Fdx=fluorescein-dextran, FLICA=fluorochrome-labeled inhibitors of caspases, LLME=Leu-Leu-OMe, NLR=NOD-like receptor, NLRP3=NOD-like receptor pyrin domain-containing 3, PLL=poly-L-lysine, PS beads=polystyrene beads, RAW=RAW 264.7, RB=Ringer's buffer, SMS=silica microsphere, sRBC=sheep RBC

1. Correspondence: Medical Science II, Room 5608, University of Michigan Medical School, Ann Arbor, MI 48109-5620, USA. E-mail: jswan@umich.edu

Phagolysosome disruption was shown to be important for caspase-1 activation following phagocytosis of silica, alum [17], and β-amyloid [15]. Hornung et al. [17] showed that silica-induced inflammasome activation required phagocytosis. Fluorescent molecules preloaded into lysosomes were released into the cytosol following exposure to silica crystals. An inhibitor of the lysosomal protease cathepsin B reduced the amount of IL-1β secretion significantly following silica exposure, suggesting that cathepsin B released from lysosomes into cytoplasm is important for inflammasome activation. However, the role of cathepsin B is still unclear, as 2 groups have reported no difference in NLRP3 inflammasome activation following lysosome disruption in mouse cells lacking the cathepsin B gene [20, 21]. The lysotropic drug LLME also strongly activated the NLRP3 inflammasome, demonstrating that lysosome damage in the absence of particle phagocytosis can also trigger inflammasome assembly.

Although these studies showed that lysosome damage after phagocytosis of silica or alum can trigger inflammasome assembly, it remains to be determined if these particles are distinct in their ability to damage lysosomes. Quantifying the extent and frequency of lysosome damage following phagocytosis would allow lysosome damage levels induced by silica to be placed into the context of phagosome maturation in general. Once the extent and frequency of lysosome damage following silica exposure are quantified, a correlation between that and downstream inflammasome signals can be explored. Moreover, inflammasome activation and activity typically follow priming of the cell with LPS or other TLR agonists. The effects of such priming on damage responses have not been examined.

Lysosome damage could release exogenous molecules into the macrophage cytosol. Therefore, lysosome damage may facilitate the cross-presentation of exogenous antigens on the MHC class I antigen-presentation system. Macropinocytosis [22, 23] as well as phagocytosis of certain particles [24–27] increase this cross-presentation and thus may involve some degree of lysosome damage.

Here we introduce a method for analyzing lysosome integrity and demonstrate that only particles that damage lysosomes activate inflammasomes. Using a novel fluoresence microscopic technique to quantify lysosome damage in live cells, we determined that silica particles induced more lysosome damage than did other particles. Not all kinds of phagolysosome became permeable, as sRBC ghosts or PS beads induced less lysosome damage than did silica. Pretreatment of macrophages with LPS reduced the lysosome damage following phagocytosis of PS beads, SMS, and ground silica. Caspase-1 activation and IL-1β release correlated with the extent of phagolysosome damage. This therefore indicates that LPS pretreatment, which is a prerequisite for inflammasome activation, also lessons the damage caused by particles inside phagolysosomes.

MATERIALS AND METHODS

Materials

Fdx average MW, 3000 dalton, Texas-Red dextran average MW, 10,000 dalton, PBS, DMEM low glucose, RPMI 1640, FBS, and sRBCs were purchased from Invitrogen (Carlsbad, CA, USA). Purified rabbit IgG was purchased from Sigma Chemical Co. (St. Louis, MO, USA). LPS was LPS #225 *Salmonella typhurium*, purchased from List Biological Laboratories, Inc. (Campbell, CA, USA). Caspase-1 FLICA reagent was purchased from Immunochemistry Technologies LLC (Bloomington, MN, USA). IL-1β ELISA was purchased from BD Biosciences (BD OptEIA, San Jose, CA, USA). PS beads (3 μm diameter) were purchased from Polysciences, Inc. (Warrington, PA, USA). Uncoated, 3 μm oxide silica microspheres (SMS) were purchased from Microspheres-Nanospheres (Cold Spring, NY, USA). Murine rM-CSF was purchased from R&D Systems (Minneapolis, MN, USA). Dishes (35 mm) with 14 mm diameter cover glass were purchased from MatTek Corp. (Ashland, MA, USA). Fisherbrand select #1.5 cover glass was purchased from Fisher Scientific (Hampton, NH, USA). Silica crystals (MIN-U-SIL-15) were a generous gift of U.S. Silica (Berkeley Springs, WV, USA).

Bone marrow differentiation of macrophages

C57BL/6J mice were purchased from Jackson Laboratories (Bar Harbor, ME, USA; Stock Number 000664). Macrophages were cultured as in ref. [28]. Briefly, marrow was obtained from mouse femurs. Macrophages were then differentiated in DMEM with 20% FBS and 30% L cell-conditioned medium. Bone marrow cultures were differentiated for 1 week with additions of fresh differentiation medium at Days 3 and 6.

Loading of lysosomes with Fdx

Labeling lysosomes by endocytosis of Fdx has been described previously [3, 29]. Macrophages were resuspended from dishes after incubation in cold PBS for 10 min. Cells were then counted, diluted in RPMI with 10% FBS, added to coverslips or Mat-tek dishes, and allowed to attach to the glass surface for at least 4 h. Plating medium was replaced with RPMI with 10% FBS containing Fdx at 150 μg/mL, and cultures were incubated overnight. Dishes or coverslips were then rinsed extensively with RB (155 mM NaCl, 5 mM KCl, 2 mM $CaCl_2$, 1 mM $MgCl_2$, 2 mM NaH_2PO_4, 10 mM Hepes, 10 mM glucose, pH 7.2) at 37°C. The Fdx was chased into the lysosomes for at least 4 h using fresh RMPI with 10% FBS without Fdx.

Opsonization of particles

sRBC ghosts were prepared as described previously [24]. Briefly, sRBC were lysed osmotically in water, and the released contents were rinsed away by centrifugation and resuspension. Texas-Red dextran was then mixed with sRBC membranes, which were then re-sealed in osmotically balanced PBS. These sRBC ghosts were then opsonized using anti-sRBC antibody, rinsed, and counted using a hemocytometer on a fluorescence microscope. PS beads were opsonized by absorption with rabbit IgG for 30 min at 37°C, followed by rinsing in PBS.

SMS were acid-washed overnight in 1 M HCl and then rinsed three times in PBS. SMS were coated with 0.1 mg/mL PLL in PBS for 30 min, followed by another round of 3 PBS washes. PLL-coated SMS were coated in 5 mg/mL BSA for 1 h and then rinsed 3 times in PBS. SMS were opsonized with anti-BSA IgG for 1 h and then rinsed in PBS. Samples were reserved following each step for experimentation.

Microscopes and imaging

Ratiometric imaging was performed on 2 different instruments. The first was an Olympus IX70 (Olympus, Center Valley, PA, USA) inverted epi-fluorescence microscope using a 100× oil UPlan Fl objective (numerical aperture=1.30). Fluorescence images were acquired using an X-Cite 120 metal halide light source (EXFO, Mississauga, ON, Canada) and a CoolSNAP HQ2 monochrome camera (cooled CCD, 1392×1040, 14 bit). The second instrument was an inverted Nikon TE300 microscope equipped for multicolor fluorescence imaging using a mercury arc lamp. Cells were examined using a 60× numerical aperture 1.4 plan-apochromat objective, and images were recorded using a cooled digital CCD camera (Quantix Photometrics, Tucson, AZ, USA). Both microscopes used temperature-controlled stages

for live cell imaging and were equipped with CFP/YFP/DsRed dichroic mirrors (Chroma Techonology Corp., Bellows Falls, VT, USA; Cat. #86006), and filter wheels and shutters were controlled by λ 10-2 filter wheel controllers (Sutter Instruments, Novato, CA, USA).

Images were acquired and analyzed using Metamorph software (Molecular Devices, Downingtown, PA, USA), following a 1-h incubation with phagocytic targets. Cells were rinsed and mounted onto the microscope stage in warm RB. For each field of cells, 3 images were collected, using a 436/10-nm excitation (ex.), a 492/18-nm ex., and a phase-contrast image. A 535/30-nm emission filter was used for both fluorescence images. An additional image using red ex. and emission filters was acquired for cells fed sRBC ghosts containing Texas-Red dextran.

Image analysis

Epi-fluorescence images contain contaminating signals from camera background noise and uneven illumination. The level of background signal was determined by capturing images without a coverslip mounted on the stage. These values were subtracted from all experimental and calibration images. Illumination correction was performed by collecting images of an even layer of fluorophore sandwiched between two coverslips [30]. Experimental and calibration images were normalized for illumination levels. Incubation of coverglasses or Mat-tek dishes in Fdx medium, even when followed by rinsing, created residual background fluorescence. This background was subtracted from all experimental images using regions selected from noncellular portions of the experimental and calibration images [29, 30].

The pH of intracellular compartments was determined as described previously [3, 29]. The microscope was calibrated by imaging intracellular organelles held at a series of fixed pHs. Macrophages were loaded with Fdx by endocytosis, and the pH of intracellular compartments was clamped using calibration buffer (10 μM nigericin, 10 μM valinomycin, 130 mM KCl, 1 mM $MgCl_2$, 15 mM Hepes, 15 mM MES) at pH 7.5. Several sets of epifluorescence images using the 435-nm and 492-nm excitation filter settings were acquired, the calibration buffer was exchanged for buffer at another pH, and another set of images was acquired from other cells. This process was repeated using buffers at pH 9.0, 7.5, 7.0, 6.5, 6.0, 5.5, 5.0, 4.5, and 4.0. Subsequent image processing determined the average ratio of the 492-nm image divided by the 435-nm image for each pH. The data were fit to a 4-parameter sigmoid model, and this model was used to convert every Fdx-labeled pixel in the 492-nm/435-nm ratio images into values representing pH (see Fig. 1C).

In processed images of unperturbed macrophages, most pixels indicated a pH <5.5. This was determined empirically by examination of many Fdx-loaded but otherwise unperturbed cells on many different days and was true for both microscopes. Thus, cellular areas in pH maps with a pH below 5.5 were considered to represent intact lysosomes, and areas with a pH above 5.5 indicated Fdx in pH neutral cytosol.

Using cellular pH maps and image processing software, masks were created that contained only pixels indicating a pH above 5.5. These masks were applied to the otherwise unmasked 435-nm ex. images. As the fluorescence of fluorescein excited at 435 nm ex. is relatively insensitive to pH, pixel fluorescence values in 435 nm ex. images were considered to be proportional to the amount of Fdx in each pixel. Thus, the total cellular fluorescence in the 435-nm ex. image was proportional to the total Fdx in the cell, and the total cellular fluorescence in the masked 435-nm ex. image approximated the total amount of Fdx released from the lysosomes. The values of total Fdx content and total Fdx released were recorded for each cell, and the ratio of Fdx released was divided by total Fdx to obtain the fraction of Fdx released. As the fluorescence images are only masked based on pH and never masked based on fluorescence intensity, this technique does not rely on any subjective masking to define the presence or absence of lysosome damage.

It should be noted (see Figs. 1–3) that the brightness of the 492-nm ex. and 435-nm ex. gray-scale image samples is scaled identically to illustrate the differences in intensity ratios. In cells with low levels of lysosome damage, the 435-nm ex. and the 492-nm ex. image were similarly bright; however, in cases of very high levels of lysosome damage, the 492-nm ex. image was much brighter than the 435-nm ex image. Thus, identical brightness scaling can result in 435 nm ex. images, which appear dim in cases of high lysosome damage.

Caspase-1 activation levels

Levels of active caspase-1 in live cells were determined using the caspase-1 FLICA probe, which labels irreversibly the active site of cleaved (activated) caspase-1 with fluorophore. Macrophages were stimulated overnight in 100 ng/mL LPS. Cells were fed particles in fresh medium and incubated for 1 h. Particle medium was then replaced with the diluted FLICA reagent, as per the manufacturer's recommendations and incubated for 1 h. Propidium iodide was added to the staining solution for the last 10 min of the incubation. Cells were then rinsed to remove the unbound dye and imaged using the 492/18-nm ex., 535/30-nm emission filters for the active caspase-1 signal and 580/20 nm ex. and 630/60 nm emission filters for propidium iodide staining. Images were corrected for background and illumination, as described above. Regions of interest were then drawn around each cell, and the total 492/18-nm ex. and 535/30-nm emission fluorescence was calculated as the total active caspase-1 signal. The propidium iodide staining and nuclear phase-contrast status were also noted for each cell.

Statistical tests

Lysosome damage levels were compared between groups using Student's *t* test and *P* values calculated in Microsoft Excel. Error bars displayed in the figures were all SEM.

RESULTS AND DISCUSSION

Release of Fdx from lysosomes into cytoplasm

To measure lysosome damage, lysosomes were first labeled by endocytosis of Fdx. RAW macrophages were incubated overnight in Fdx-containing medium and then incubated in fresh medium to allow the Fdx to reach the lysosomes by vesicular trafficking. Ratiometric imaging with a calibrated microscope was then used to measure the pH of cytoplasmic and lysosomal Fdx (**Fig. 1C** is a sample calibration curve). Fdx fluorescence (514 nm) was imaged at 2 different excitation wavelengths. Excitation at 435 nm produced fluorescence that was relatively unaffected by pH, which was used to approximate the amount of Fdx in a pixel, whereas ex. at 492 nm produced a pH-dependent fluorescence. Release of Fdx from lysosomes into cytosol was detected by the physical redistribution of the dye in the images and by the increase in Fdx signal at 492 nm excitation. pH maps of cells provided a clear distinction between Fdx trapped in acidic, undamaged lysosomes and Fdx, which had been released into the pH-neutral cytosol. Fdx in unperturbed macrophages was contained in acidic lysosomes (Fig. 1A). In similarly loaded macrophages exposed to the lysotropic drug LLME, Fdx was released into the cytosol (Fig. 1B and D). LLME disrupted all of the lysosomes in RAW macrophages, as the pH map of these cells appeared uniform and neutral (Fig. 1B and D). To quantify lower levels of Fdx release from lysosomes, image analysis algorithms were developed to measure the percentage of total cellular Fdx in the cytoplasm (Fig. 1D).

Undisturbed BMM show little lysosome damage

BMM contained spherical and elongated tubular lysosomes. The areas of highest lysosome density were near the nuclei,

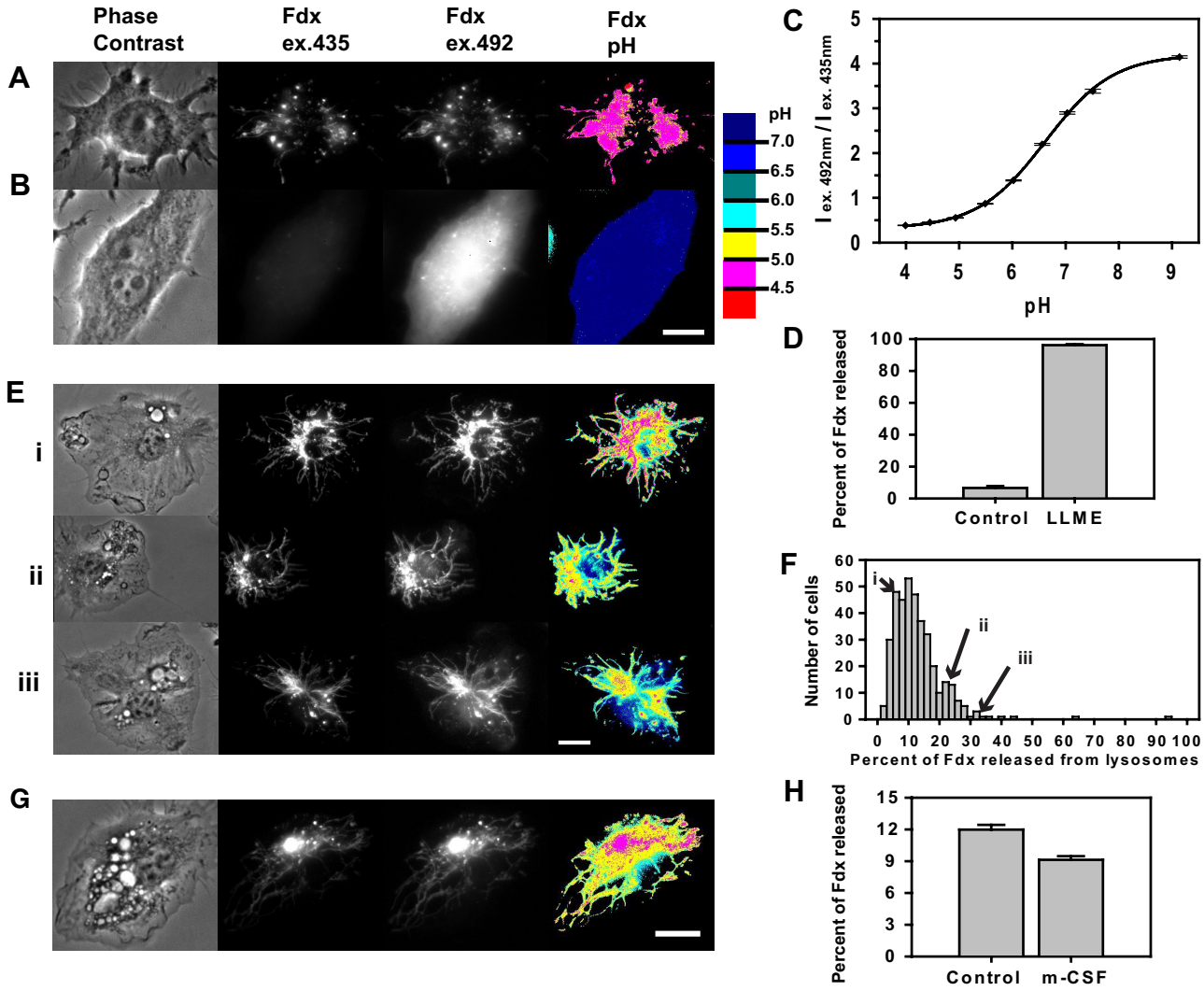

Figure 1. Detection of Fdx released from lysosomes. RAW macrophage lysosomes were loaded overnight with Fdx and then chased for several hours in fresh medium. Cells were left untreated (A) or incubated with LLME for 30 min (B), and then epi-fluorescence images were collected. All pH images are color-coded such that warm colors (red, pink, and yellow) represent Fdx in acidic compartments, and cool colors (cyan, dark cyan, blue, and dark blue) represent Fdx in pH neutral compartments. Ratios (ex. 492 nm:ex. 435 nm) were converted to pH using calibration curves generated by measuring ex. 492 nm:ex. 435 ratios at fixed pHs (C). The brightness of the Fdx ex. 435 nm and ex. 492 nm images is scaled identically in all micrograph sets. (D) The percentage of Fdx released from the lysosomes is plotted as mean ± SEM of ≥70 cells ($P<0.0001$). BMM were loaded and imaged as above. (E) Epi-fluorescence images of otherwise unperturbed macrophages were then collected. Images of unperturbed cells depicting very low (i, 7.7%), slight (ii, 22.4%), and moderate (iii, 31.6%) lysosome release. (F) Lysosome release from all of the negative control images acquired for G and see Fig. 2. (G) Typical images of BMM following M-CSF-induced macropinocytosis. Original scale bars represent 10 μm. (H) Lysosome release from all of the cells in each group was calculated and the averages plotted. Error bars are SEM. Data are pooled averages of 3 experiments; $n \geq 200$ cells total; $P < 0.0001$.

and tubular structures extended into the periphery (Fig. 1E, i), consistent with previous observations [31]. Lysosomal pH was 4.0–5.0, as reported previously [3, 32]. Unperturbed macrophages showed little evidence of lysosome damage (Fig. 1E, i, and F). Most pixels in the pH maps of intact cells represented acidic environments. A few cells displayed higher levels of lysosome damage (Fig. 1E, ii and iii).

Rare cells exhibited low levels of lysosome damage in otherwise unperturbed cells. Although many of the pH neutral pixels were dim, their intensity in the 435-nm images was several times greater than the noise level. Nuclear regions were the best cellular locations to detect low levels of released Fdx, as those regions contained no fluorescence from lysosomes. The low levels of Fdx in the cytosol of these cells produced undetectable signals in the periphery.

Increasing the rate of macropinocytosis does not increase lysosome damage

The low level of damage in unperturbed macrophages suggested that some basic cellular process can damage lysosomes.

Macropinocytosis is the process by which macrophages and other cells take up extracellular solute into large endocytic vacuoles. Solutes taken into macropinosomes traffic through the endocytic pathway, eventually entering lysosomes [32]. M-CSF increases the rate of macropinocytosis in macrophages [33]. Induction of macropinocytois in macrophages increases cross-presentation of soluble exogenous antigens on MHC class I molecules [22, 23].

To measure effects of macropinocytosis on lysosome damage, macrophage lysosomes were loaded with Fdx in cells deprived of M-CSF, chased in Fdx-free medium, and incubated 1 h in medium containing M-CSF or control medium before imaging. Cells incubated in M-CSF displayed prominent macropinosomes (Fig. 1G, Phase Contrast). Lysosome damage in cells exposed to M-CSF was no greater than in control cells (Fig. 1H), indicating that macropinocytosis-mediated increases in soluble antigen cross-presentation in macrophages [22] are not a result of increased lysosome damage following macropinocytosis.

Lysosome damage following phagocytosis

To examine whether lysosome damage is a general outcome of phagocytosis, macrophages with Fdx-labeled lysosomes were fed Texas-Red dextran-labeled sRBC ghosts. Fluorescent sRBC ghosts were imaged 1 h after phagocytosis, and levels of Fdx release from lysosomes were quantified (**Fig. 2**). Phagocytosis of sRBC ghosts induced a redistribution of macrophage lysosomes to phagosomes (Fig. 2B), consistent with previous observations [31]. In cells containing several sRBC ghosts, nearly all of the phagolysosomes coalesced into large, round structures containing the sRBC ghosts and most of the cellular Fdx. Despite this dramatic redistribution, no additional lysosome damage followed phagocytosis of sRBC ghosts (Fig. 2E).

The Fdx-release assay was used to measure phagolysosome damage by various particles. Macrophages fed ground silica showed extensive phagolysosome damage (Fig. 2D). In some ground silica-containing cells, lysosome damage was evident without the aid of the pH map, and in other cells, no damage was detected. Most silica-fed macrophages showed intermediate levels of lysosome damage, with Fdx in cytosol and intact lysosomes.

The highly variable lysosome damage in cells containing ground silica contrasts with LLME-treated cells, which exhibited complete lysosome release in all cells. The lack of uniformity in cells fed silica could be a result of some nonuniform aspect of these particles, such that only some of them were disruptive. Perhaps not all particles possess sharp edges that cause damage. Alternatively, resistance to lysosome perforation may be regulated, and the nonuniformity in lysosome release could be the result of different gene expression patterns in different cells of the examined populations.

Fdx-loaded macrophages were also fed 3 μm PS beads, which are widely used as inert phagocytic targets. PS beads

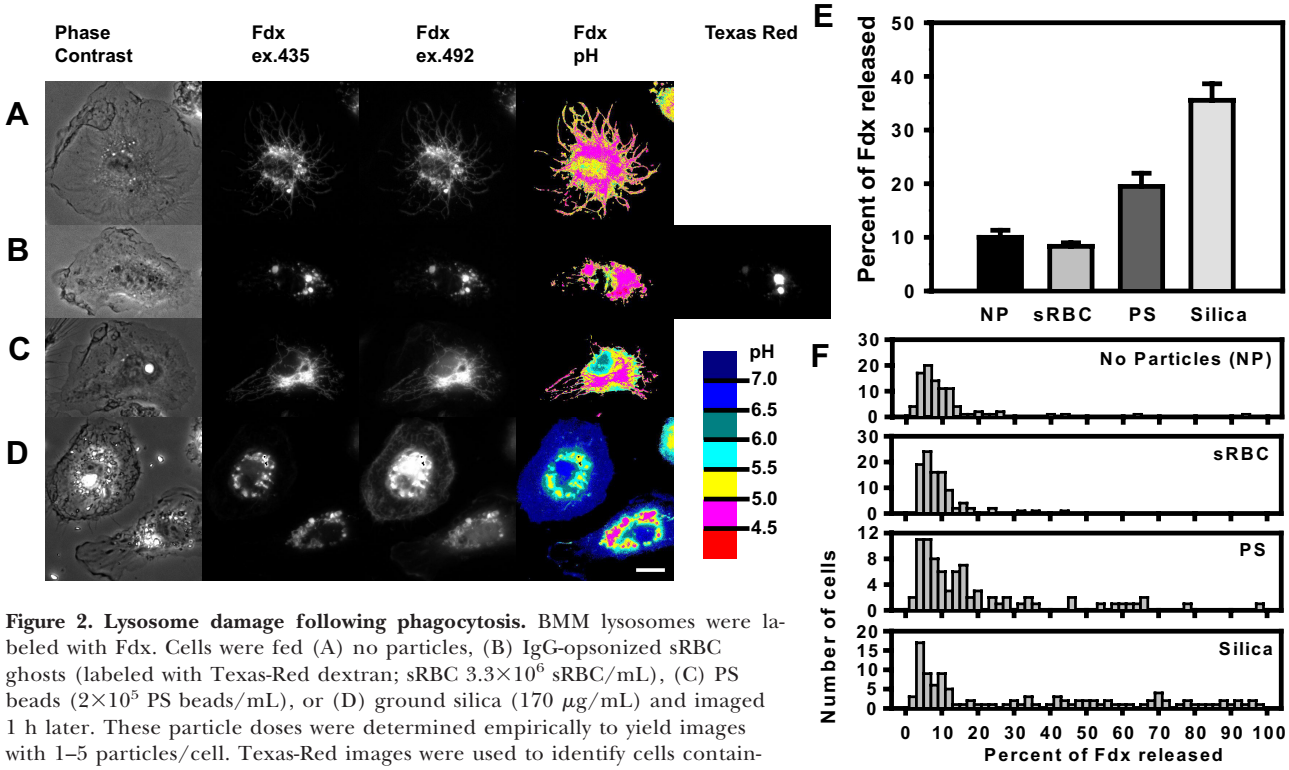

Figure 2. Lysosome damage following phagocytosis. BMM lysosomes were labeled with Fdx. Cells were fed (A) no particles, (B) IgG-opsonized sRBC ghosts (labeled with Texas-Red dextran; sRBC 3.3×10^6 sRBC/mL), (C) PS beads (2×10^5 PS beads/mL), or (D) ground silica (170 μg/mL) and imaged 1 h later. These particle doses were determined empirically to yield images with 1–5 particles/cell. Texas-Red images were used to identify cells containing sRBC ghosts. Original scale bar represents 10 μm. (E) The average percent of lysosome release was calculated for each condition. Data represent mean ± SEM for 3 separate experiments with at least 80 cells examined in each condition. All conditions are significantly different ($P<0.0005$) from each other, except for no particle (NP) versus sRBC ghost. (F) The data from E, replotted as histograms, with percent of Fdx released (*x*-axis) compared with the number of cells containing a given level of Fdx release (*y*-axis).

were shown earlier to facilitate the delivery of exogenous antigens into the MHC class I antigen processing and presentation pathways [24], suggesting that they induce damage at some stage of their endocytic trafficking. Other types of microspheres have also been shown to facilitate exogenous antigen presentation on MHC class I molecules [25–27]. The amount of Fdx released into the cytosol of PS bead-containing macrophages was significantly greater than in unfed cells or cells fed sRBC ghosts but less than that released in cells fed ground silica (Fig. 2E and F). Thus, phagocytosis of particles yields a range of lysosome damage dependent on dosage and the type of particle phagocytosed.

The heterogeneity among cells showing lysosome damage may have implications for cross-presentation of exogenous antigens on MHC class I molecules. The subpopulation of cells showing lysosome release in unperturbed cultures could represent those that have released exogenous antigens into the cytosol, which would then be accessible to the MHC class I antigen presentation pathway. This could underlie the low but detectable level of cross-presentation of soluble antigens observed in macrophages [22, 25, 27, 34]. Although macropinocytosis did not increase lysosome damage in macrophages, increased uptake of soluble antigen into cells could nonetheless mediate increased cross-presentation of soluble antigens in the small fraction of cells that undergo lysosome damage. PS beads fed to unactivated macrophages induced low but detectable levels of damage, which may explain the reported cross-presentation of antigens loaded onto PS beads [24]. The release of lysosomal contents after PS bead phagocytosis supports a direct mechanical route for antigen delivery into the cytosol for MHC class I antigen presentation.

LPS reduces the phagolysosome damage

Recent studies have shown that lysosome damage can induce maturation and secretion of the proinflammatory cytokine IL-1β [15, 17], and IL-1β secretion from murine macrophages requires prestimulation with a TLR ligand such as LPS. Prestimulation of LPS is required for transcription and translation of pro-IL-1β [12] and NLRP3 [35], as well as many other changes in gene expression.

To investigate whether these physiologic changes modulate lysosome damage, the damage induced by various particles was compared in LPS-activated and untreated control macrophages, and macrophage lysosomes were loaded with Fdx in medium, with or without LPS, and the cells were fed particulate targets. LPS treatment did not alter lysosomal pH. Fdx release after phagocytosis of ground silica was less in LPS-stimulated macrophages than in unstimulated macrophages (**Fig. 3A**). LPS treatment also decreased lysosome damage following phagocytosis of PS beads to levels that were significantly lower than in untreated cells fed similar doses of beads (Fig. 3B, 1.5 PS beads/cell). This relationship was also evident in macrophages fed higher doses of PS beads (Fig. 3B, 18.3 PS beads/cell). These data indicate that lysosome damage may be modulated by the activation state of the macrophages.

To confirm that LPS prestimulation reduces lysosome damage, SMS were used. SMS are uniform, 3 μm spheres that are chemically similar to the ground silica. This uniformity of size and shape allowed for particle dose to be determined independently for each cell. Acid-washed SMS were coated with various materials and then fed to Fdx-loaded macrophages, which had or had not been prestimulated with LPS. The num-

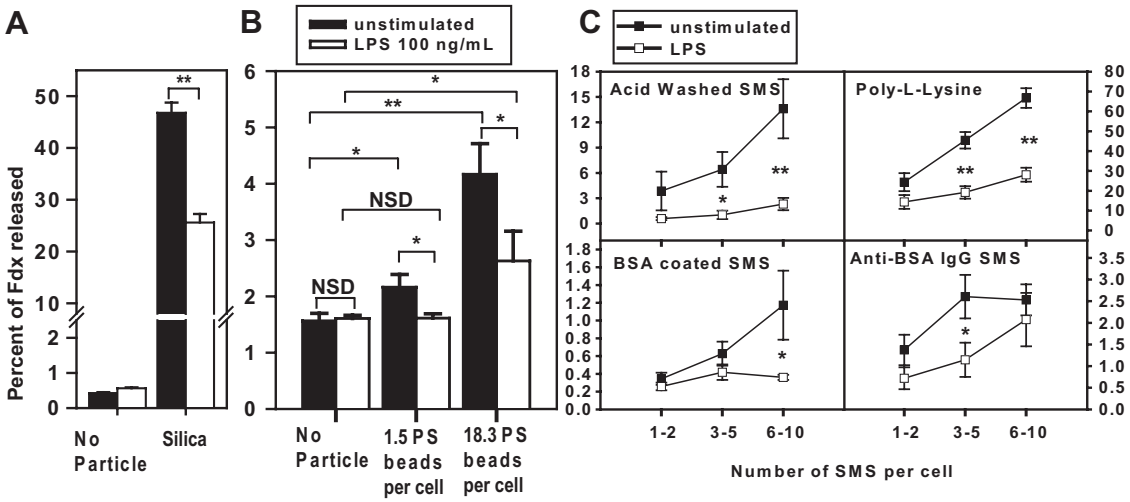

Figure 3. LPS treatment decreases lysosome release following phagocytosis. BMM were labeled with Fdx and chased in unlabeled medium with (open bars) or without (closed bars) 100 ng/mL LPS. Cells were fed particles and imaged, and the average percent of lysosome release was calculated for each condition. *y*-Axis for all graphs plot the average percent of Fdx released. (A) LPS-stimulated or naïve BMM were fed 200 μg/mL ground silica, and lysosome damage was measured. (B) The number of PS beads/cell was counted and indicated for each PS bead dose. (A and B) Bars are pooled averages from 3 experiments with at least 170 cells/condition (means±SEM). (C) Cells were fed acid-washed SMS coated with nothing (upper left), PLL (upper right), BSA (lower left), or BSA and anti-BSA IgG (lower right). Cells were imaged, and the number of phagocytosed SMS was recorded for each cell. Cells were grouped by number of SMS phagocytosed, and mean ± SEM was plotted for each group. Statistical comparisons in A and B are as indicated with brackets and in C are between unstimulated and LPS-prestimulated groups within each SMS type and count. *P* values: NSD, Not significantly different; $*P < 0.05$; $**P < 0.0001$.

ber of SMS internalized by each cell was counted, and populations of cells that had phagocytosed the same dose of particles were compared. Macrophages fed acid-washed SMS showed moderate levels of lysosome damage (Fig. 3C). Phagocytosis of PLL-coated SMS induced high levels of lysosome damage, and SMS coated with BSA or BSA and anti-BSA IgG induced lower levels of lysosome damage (Fig. 3C), which was dose-dependent. LPS prestimulation reduced lysosome damage for all SMS coatings and all dose levels (Fig. 3C). These data confirmed that LPS prestimulation reduces lysosome damage following particle phagocytosis. Experiments with SMS suggested that particle surface chemistry may play an important role in inducing lysosome damage, as the SMS with different surface treatments damaged lysosomes to different extents. Thus, lysosome damage was not intrinsic to phagocytosis but rather, was a result of surface features of the ingested particles.

Lysosome damage correlates with caspase-1 activation

To determine if inflammasome activation was proportional to lysosome damage, caspase-1 activation was measured in macrophages fed various particles. Cells were stained with the fluorescent caspase-1 reporter FLICA, which labels the active site of cleaved caspase-1 in live cells (**Fig. 4A**). The percent of cells positive for caspase-1 activation increased with increasing doses of silica (Fig. 4B and **Table 1**). Most caspase-1-positive cells were also positive for propidium iodide (90–96%; Table 1 and

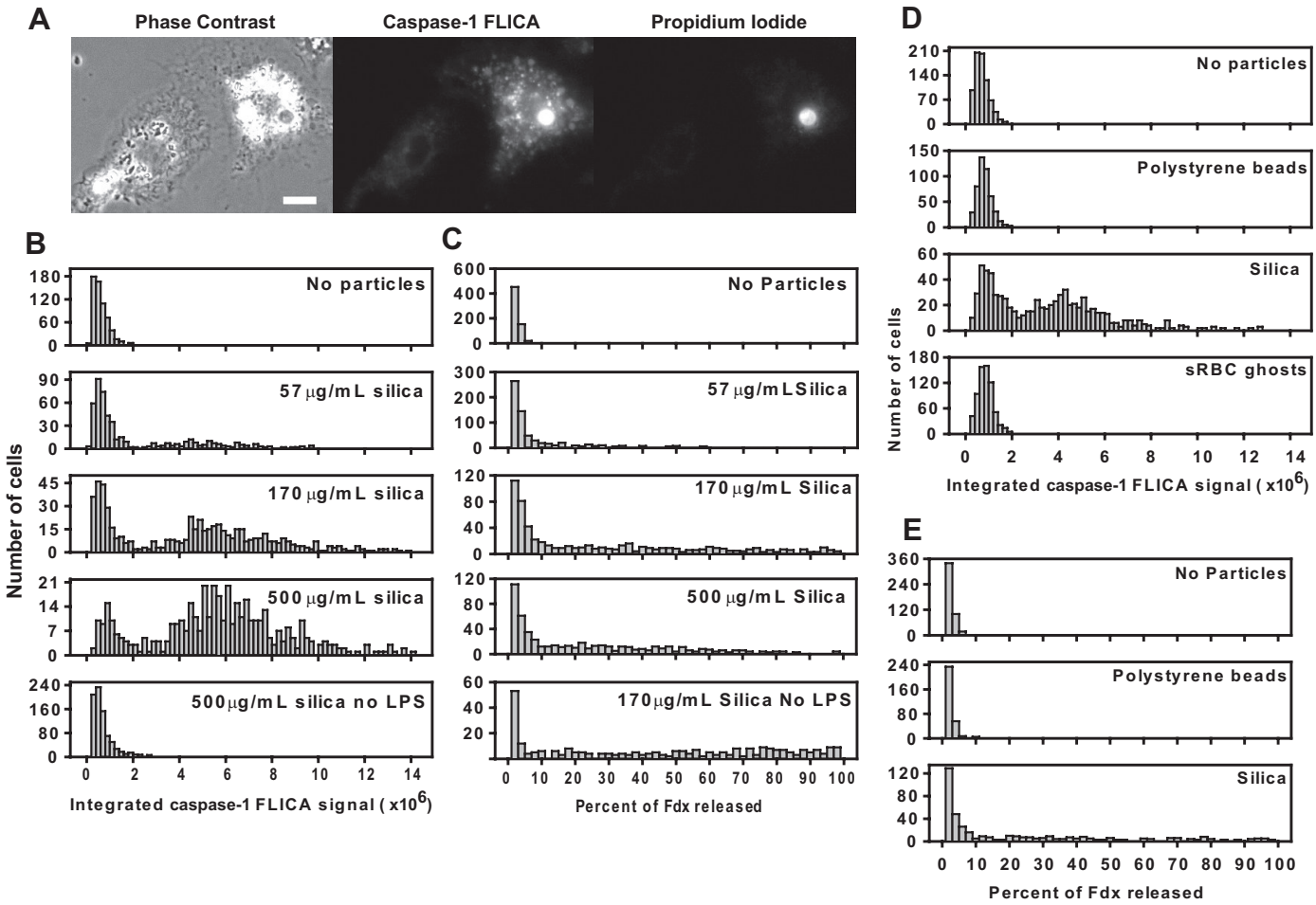

Figure 4. Caspase-1 activation correlates with lysosome damage. BMM were treated overnight with or without LPS and then fed ground silica at 57, 170, or 500 μg/mL or were left unfed (No particles). (A and B) Cells were then stained for an additional 1 h using the caspase-1 FLICA reagent; propidium iodide was added for the last 10 min to detect cells with permeabilized plasma membranes. Active caspase-1 (FLICA) and propidium iodide were imaged and quantified. (A) Sample images of LPS-pretreated cells fed 170 μg/mL ground silica. The cell on the right shows high levels of caspase-1 activation detected by FLICA, nuclear propidium iodide staining, and a phase-dark nucleus, and the cell on the left contains silica but is negative for FLICA, propidium iodide, and nuclear condensation. Original scale bar represents 10 μm. (B) Data are displayed as histograms with an integrated FLICA signal for individual cells plotted on the horizontal axis. (C) BMM lysosomes were labeled with Fdx in LPS-containing medium. Macrophages were fed silica as above and imaged 1 h later. Data are the pooled results of three independent experiments ($n \geq 400$ total cells/condition). (D) BMM treated with LPS were fed nothing (No particles), PS beads, ground silica, or sRBC ghosts for 1 h and then stained for active caspase-1. Histograms show integrated caspase-1 FLICA signal for individual cells plotted on the horizontal axis. Data are pooled results of three independent experiments with at least 400 total cells examined per condition. (E) Data from LPS-prestimulated BMM are replotted as histograms for comparison with D.

TABLE 1. Compiled Numerical Data

Particle	Dose	Lysosome release			Caspase-1 activation					IL-1β secretion
		% of Cells positive for LD	% of Cells positive for LD or PDN	% of Fdx released	% of Cells positive for FLICA	Mean FLICA fluorescence intensity	% of Cells positive for PI	% of FLICA + cells that were PI+	% of FLICA + cells that were PDN+	pg/mL
No Particles	0	0	0	2	0	5.9E + 05	1	†	†	2
sRBC ghosts	2.5 ghosts/cell	ND	ND	ND	1	7.8E + 05	0	†	†	1
PS beads	1.5 beads/cell	0	0	2	1	7.4E + 05	0	†	†	1
PS beads	18.3 beads/cell	2	2	3	ND	ND	ND	ND	ND	95
Silica	57 μg/mL	29	30	14	32	2.2E + 06	32	90	98	772
Silica	170 μg/mL	50	54	28	64	4.0E + 06	66	96	96	1309
Silica	500 μg/mL	56	65	30	85	5.8E + 06	88	97	98	1537
Silica No LPS	170 μg/mL	45	45	28	ND	ND	ND	ND	ND	ND
Silica No LPS	500 μg/mL	ND	ND	ND	9	9.8E + 05	6	69	70	0

Data are from LPS-stimulated BMM, except where noted. Cells with lysosome release <10% and with caspase-1 FLICA signal >2 × 10^6 fluorescence units were considered positive for lysosome damage and caspase-1 activation, respectively. LD, Lysosome damage; PDN, phase-dark nuclear morphology; PI, propidium iodide; †, sample size is small (<10 FLICA-positive cells); ND, conditions for which there are no data.

Fig. 4A), indicating plasma membrane permeabilization. This FLICA-positive, propidium iodide-positive population also exhibited phase-dark nuclear morphologies indicative of cell death (Fig. 4A and Table 1). Caspase-1 activation was LPS-dependent, as even high doses of silica failed to induce FLICA staining in unstimulated cells (Fig. 4B, bottom panel). The percent of cells positive for lysosome damage also increased with increasing doses of silica (Fig. 4C). The average level of lysosome release observed at 500 μg/mL silica was not greater than that observed at 170 μg/mL. However, macrophages fed the higher doses of silica contained many more cells with phase-dark nuclei than did those fed intermediate doses (Table 1), and cells with phase-dark nuclei did not retain sufficient Fdx to allow the lysosome release analysis. Measurements of IL-1β release indicated a correlation between IL-1β secretion and the amount of silica provided to cells (**Fig. 5A**). Overall, lysosome damage, caspase-1 activation, and IL-1β secretion showed large increases between 57 and 170 μg/mL silica and leveled off between 170 and 500 μg/mL.

Thus, in activated macrophages, various doses of silica showed corresponding percentages of lysosome damage, caspase-1 activation, and secretion of IL-1β, suggesting a pattern of progression to inflammasome activation following silica phagocytosis. In silica-fed macrophages, inflammasome activation was accompanied by loss of plasma membrane integrity and nuclear condensation. These data suggest a role for cell death in the silica-induced lysosome damage response, possibly

Figure 5. Secretion of IL-1β following particle phagocytosis is proportional to lysosome damage. BMM pretreated with LPS were fed opsonized sRBC ghosts, PS beads, or silica. After 4 h, culture supernatants were harvested and analyzed for IL-1β content. Data are averaged results from 3 independent experiments.

through pyroptosis [36]. LPS prestimulation was critical for cell death, as unstimulated cells fed lysosome-damaging doses of silica failed to activate caspase-1 or to lose plasma membrane integrity. The staining protocols precluded measurement of the relative timing of caspase-1 activation, membrane permeabilization, and nuclear condensation.

The lysosome damage induced by PS beads did not induce IL-1β release

The lack of lysosome damage in LPS-stimulated cells fed PS beads suggested that caspase-1 activation and IL-1β secretion in such cells should also be low. Macrophages fed PS beads or sRBC ghosts showed low levels of caspase-1 activation (Fig. 4D). In contrast, macrophages fed silica exhibited high levels of caspase-1 activation. These data correlated with the IL-1β secretion data, in that LPS-activated macrophages fed PS beads failed to secrete IL-1β (Fig. 5A and B). Thus, IL-1β secretion and caspase-1 activation in LPS-activated macrophages fed PS beads correlated with the low levels of lysosome damage in such cells. Similar relationships were observed in cells fed higher doses of beads: LPS-activated macrophages that ingested an average of 18.3 PS beads/cell displayed little lysosome damage (Fig. 3B) and secreted little IL-1β (Fig. 5B). These data indicate that LPS stimulation interferes with or counteracts lysosome damage after phagocytosis of PS beads.

Previous work showed that silica, alum [17], and β-amyloid [15] damage lysosomes. In contrast, this study found that macrophages fed sRBC ghosts showed lysosome release levels no higher than control cells (Fig. 2), and cells fed PS beads, another classic phagocytic target, showed low levels of lysosome damage, which were higher than control cells or cells fed sRBC ghosts but lower than cells fed silica. Although SMS phagocytosis seemed to damage lysosomes to a lesser extent than did ground silica, direct comparisons were difficult as a result of irregularities of the ground silica particle shape and size.

Some bacterial pathogens escape from macrophage vacuoles to propagate in the host cell cytosol. The macrophage IL-1β response to *Listeria monocytogenes* is partially dependent on NLRP3 and bacterial escape [37], suggesting that the escape process damages lysosomes. On the other hand, *Francisella tularensis* escapes from vacuoles but does not activate the NLRP3 inflammasome [38]. These data may reflect differences in the vacuolar compartments from which these bacteria escape or the severity of lysosome damage induced during escape.

LPS-stimulated cells fed ground silica, PS beads, or SMS showed less lysosome damage than unstimulated cells (Fig. 4), suggesting that LPS-activated cells are refractory to damage induced by particles or that there exists a mechanism for lysosomal repair, which is increased by LPS prestimulation. The LPS-dependent phagolysosome damage-resistance activity is limited, as particles that cause high amounts of lysosome damage, such as ground silica and PLL-coated SMS, still induce significant levels of phagolysosome damage in LPS-stimulated cells. As prestimulation with LPS or other TLR ligands is critical for inflammasome activation following lysosome damage, as a result of the dependence of NLRP3 expression on prestimulation [35], the dampening effect of LPS on phagolysosome damage seems to counteract inflammasome activation after phagocytosis. It remains to be seen whether the inflammasome gene expression effects can be separated from the lysosome-stabilizing effects of LPS signaling. Although inflammasome induction by LPS requires gene expression, it is unknown whether the phagolysosome-protecting activities also require induced gene expression. Perhaps the inflammasome gene expression signals can be separated from the phagolysosome protective signals. As other solid particles are known to mediate the cross-presentation of antigens [25–27], it is possible that these other particles also modulate levels of lysosome damage.

AUTHORSHIP

M.J.D. performed all experimentation and data analysis and authored this text. J.A.S. was the principal investigator on this project and provided guidance and advice for all experiments and writing.

ACKNOWLEDGMENTS

This work was supported by grants to J.A.S. from the National Institutes of Health, National Institute of Allergy and Infectious Diseases. M.J.D. was supported by the Cellular Biotechnology Training Program at the University of Michigan.

REFERENCES

1. Scott, C. C., Botelho, R. J., Grinstein, S. (2003) Phagosome maturation: a few bugs in the system. *J. Membr. Biol.* **193,** 137–152.
2. Kinchen, J. M., Ravichandran, K. S. (2008) Phagosome maturation: going through the acid test. *Nat. Rev. Mol. Cell Biol.* **9,** 781–795.
3. Christensen, K. A., Myers, J. T., Swanson, J. A. (2002) pH-Dependent regulation of lysosomal calcium in macrophages. *J. Cell Sci.* **115,** 599–607.
4. Burgdorf, S., Kurts, C. (2008) Endocytosis mechanisms and the cell biology of antigen presentation. *Curr. Opin. Immunol.* **20,** 89–95.
5. Ray, K., Marteyn, B., Sansonetti, P. J., Tang, C. M. (2009) Life on the inside: the intracellular lifestyle of cytosolic bacteria. *Nat. Rev. Microbiol.* **7,** 333–340.
6. Martinon, F., Burns, K., Tschopp, J. (2002) The inflammasome: a molecular platform triggering activation of inflammatory caspases and processing of proIL-β. *Mol. Cell* **10,** 417–426.
7. Martinon, F., Mayor, A., Tschopp, J. (2009) The inflammasomes: guardians of the body. *Annu. Rev. Immunol.* **27,** 229–265.
8. Eder, C. (2009) Mechanisms of interleukin-1β release. *Immunobiology* **214,** 543–553.
9. Thornberry, N. A., Bull, H. G., Calaycay, J. R., Chapman, K. T., Howard, A. D., Kostura, M. J., Miller, D. K., Molineaux, S. M., Weidner, J. R., Aunins, J., et al. (1992) A novel heterodimeric cysteine protease is required for interleukin-1 β processing in monocytes. *Nature* **356,** 768–774.
10. Dinarello, C. A. (2009) Immunological and inflammatory functions of the interleukin-1 family. *Annu. Rev. Immunol.* **27,** 519–550.
11. Martinon, F., Petrilli, V., Mayor, A., Tardivel, A., Tschopp, J. (2006) Gout-associated uric acid crystals activate the NALP3 inflammasome. *Nature* **440,** 237–241.
12. Mariathasan, S., Weiss, D. S., Newton, K., McBride, J., O'Rourke, K., Roose-Girma, M., Lee, W. P., Weinrauch, Y., Monack, D. M., Dixit, V. M. (2006) Cryopyrin activates the inflammasome in response to toxins and ATP. *Nature* **440,** 228–232.
13. Perregaux, D., Gabel, C. A. (1994) Interleukin-1 β maturation and release in response to ATP and nigericin. Evidence that potassium depletion mediated by these agents is a necessary and common feature of their activity. *J. Biol. Chem.* **269,** 15195–15203.
14. Dostert, C., Petrilli, V., Van Bruggen, R., Steele, C., Mossman, B. T., Tschopp, J. (2008) Innate immune activation through Nalp3 inflammasome sensing of asbestos and silica. *Science* **320,** 674–677.
15. Halle, A., Hornung, V., Petzold, G. C., Stewart, C. R., Monks, B. G., Reinheckel, T., Fitzgerald, K. A., Latz, E., Moore, K. J., Golenbock, D. T. (2008) The NALP3 inflammasome is involved in the innate immune response to amyloid-β. *Nat. Immunol.* **9,** 857–865.

16. Cassel, S. L., Eisenbarth, S. C., Iyer, S. S., Sadler, J. J., Colegio, O. R., Tephly, L. A., Carter, A. B., Rothman, P. B., Flavell, R. A., Sutterwala, F. S. (2008) The Nalp3 inflammasome is essential for the development of silicosis. *Proc. Natl. Acad. Sci. USA* **105,** 9035–9040.
17. Hornung, V., Bauernfeind, F., Halle, A., Samstad, E. O., Kono, H., Rock, K. L., Fitzgerald, K. A., Latz, E. (2008) Silica crystals and aluminum salts activate the NALP3 inflammasome through phagosomal destabilization. *Nat. Immunol.* **9,** 847–856.
18. Eisenbarth, S. C., Colegio, O. R., O'Connor, W., Sutterwala, F. S., Flavell, R. A. (2008) Crucial role for the Nalp3 inflammasome in the immunostimulatory properties of aluminium adjuvants. *Nature* **453,** 1122–1126.
19. Petrilli, V., Papin, S., Dostert, C., Mayor, A., Martinon, F., Tschopp, J. (2007) Activation of the NALP3 inflammasome is triggered by low intracellular potassium concentration. *Cell Death Differ.* **14,** 1583–1589.
20. Dostert, C., Guarda, G., Romero, J. F., Menu, P., Gross, O., Tardivel, A., Suva, M. L., Stehle, J. C., Kopf, M., Stamenkovic, I., Corradin, G., Tschopp, J. (2009) Malarial hemozoin is a Nalp3 inflammasome activating danger signal. *PLoS One* **4,** e6510.
21. Newman, Z. L., Leppla, S. H., Moayeri, M. (2009) CA-074Me protection against anthrax lethal toxin. *Infect. Immun.* **77,** 4327–4336.
22. Norbury, C. C., Hewlett, L. J., Prescott, A. R., Shastri, N., Watts, C. (1995) Class I MHC presentation of exogenous soluble antigen via macropinocytosis in bone marrow macrophages. *Immunity* **3,** 783–791.
23. Rock, K. L., Rothstein, L., Fleischacker, C., Gamble, S. (1992) Inhibition of class I and class II MHC-restricted antigen presentation by cytotoxic T lymphocytes specific for an exogenous antigen. *J. Immunol.* **148,** 3028–3033.
24. Oh, Y. K., Harding, C. V., Swanson, J. A. (1997) The efficiency of antigen delivery from macrophage phagosomes into cytoplasm for MHC class I-restricted antigen presentation. *Vaccine* **15,** 511–518.
25. Kovacsovics-Bankowski, M., Clark, K., Benacerraf, B., Rock, K. L. (1993) Efficient major histocompatibility complex class I presentation of exogenous antigen upon phagocytosis by macrophages. *Proc. Natl. Acad. Sci. USA* **90,** 4942–4946.
26. Harding, C. V., Song, R. (1994) Phagocytic processing of exogenous particulate antigens by macrophages for presentation by class I MHC molecules. *J. Immunol.* **153,** 4925–4933.
27. Reis e Sousa, C., Germain, R. N. (1995) Major histocompatibility complex class I presentation of peptides derived from soluble exogenous antigen by a subset of cells engaged in phagocytosis. *J. Exp. Med.* **182,** 841–851.
28. Swanson, J. A. (1989) Phorbol esters stimulate macropinocytosis and solute flow through macrophages. *J. Cell Sci.* **94,** 135–142.
29. Shaughnessy, L. M., Hoppe, A. D., Christensen, K. A., Swanson, J. A. (2006) Membrane perforations inhibit lysosome fusion by altering pH and calcium in *Listeria monocytogenes* vacuoles. *Cell. Microbiol.* **8,** 781–792.
30. Hoppe, A., Christensen, K., Swanson, J. A. (2002) Fluorescence resonance energy transfer-based stoichiometry in living cells. *Biophys. J.* **83,** 3652–3664.
31. Knapp, P. E., Swanson, J. A. (1990) Plasticity of the tubular lysosomal compartment in macrophages. *J. Cell Sci.* **95,** 433–439.
32. Tsang, A. W., Oestergaard, K., Myers, J. T., Swanson, J. A. (2000) Altered membrane trafficking in activated bone marrow-derived macrophages. *J. Leukoc. Biol.* **68,** 487–494.
33. Racoosin, E. L., Swanson, J. A. (1989) Macrophage colony-stimulating factor (rM-CSF) stimulates pinocytosis in bone marrow-derived macrophages. *J. Exp. Med.* **170,** 1635–1648.
34. Rock, K. L., Rothstein, L., Gamble, S., Fleischacker, C. (1993) Characterization of antigen-presenting cells that present exogenous antigens in association with class I MHC molecules. *J. Immunol.* **150,** 438–446.
35. Sutterwala, F. S., Ogura, Y., Szczepanik, M., Lara-Tejero, M., Lichtenberger, G. S., Grant, E. P., Bertin, J., Coyle, A. J., Galan, J. E., Askenase, P. W., Flavell, R. A. (2006) Critical role for NALP3/CIAS1/cryopyrin in innate and adaptive immunity through its regulation of caspase-1. *Immunity* **24,** 317–327.
36. Ting, J. P., Willingham, S. B., Bergstralh, D. T. (2008) NLRs at the intersection of cell death and immunity. *Nat. Rev. Immunol.* **8,** 372–379.
37. Warren, S. E., Mao, D. P., Rodriguez, A. E., Miao, E. A., Aderem, A. (2008) Multiple Nod-like receptors activate caspase 1 during *Listeria monocytogenes* infection. *J. Immunol.* **180,** 7558–7564.
38. Fernandes-Alnemri, T., Yu, J. W., Juliana, C., Solorzano, L., Kang, S., Wu, J., Datta, P., McCormick, M., Huang, L., McDermott, E., Eisenlohr, L., Landel, C. P., Alnemri, E. S. (2010) The AIM2 inflammasome is critical for innate immunity to *Francisella tularensis*. *Nat. Immunol.* **11,** 385–393.

KEY WORDS:
pH · microscopy · phagocytosis